Proceedings of the Canadian Society for Mechanical Engineering International Congress
32nd Annual Conference of the Computational Fluid Dynamics Society of Canada
Canadian Society of Rheology Symposium
CSME/CFDSC/CSR 2025
May 25–28, 2025, Montréal, Québec, Canada

NUMBER

Buoyant miscible suspension fluid injection into a closed-end pipe

Mohsen Faramarzi[1], Seyed Mohammad Taghavi[1*]

[1]Department of Chemical Engineering, Université Laval, Québec, QC Canada G1V 0A6

January 31, 2025

***Abstract*—**This study experimentally investigates the injection of a buoyant miscible suspension into a prefilled Newtonian fluid within a closed-end pipe, where the two fluids form a miscible configuration. The experiments are conducted using an industrially scaled-down dump-bailing setup, used for cementing oil and gas wells. A high-speed camera captures the experiments, and flow parameters are extracted through image post-processing. Motivated by industrial applications, we examine the effects of initial particle volume fraction, inclination angle, and injection rate to analyze various flow patterns and assess the impact of these parameters on the quality of suspension placement, as quantified by a mixing index. The results show that reducing the inclination angle and injection rate improves placement efficiency. However, changes in the initial particle volume fraction lead to improved placement efficiency in the short term but degrade placement quality over the long term. This study offers valuable insights for cementing operations, including dump-bailing, primary cementing, hydrocarbon production, and wellbore decommissioning in oil and gas wells.

***Keywords-component*—suspension; particle-laden flow; buoyant miscible injection; oil and gas wells cementing**

I. INTRODUCTION

Displacement flows are observed in both natural systems and a wide range of industrial applications, including microfluidic devices [1], 3D printing [2], food processing [3], and the oil and gas industry [4]–[11]. In the oil and gas sector, a critical application of displacement flow is found in cementing operations, particularly during the plug and abandonment (P&A) of oil and gas wells. In cemening proceses, accurate placement of cement slurries, plugs, or alternative sealing materials at designated intervals within the wellbore is essential for mitigating environmental concerns, including greenhouse gas emissions, groundwater contamination, and ecological damage during the decommissioning of aging wells [12]–[14].

The success of such operations depends on various parameters, including the wellbore configuration and trajectory, conditions in the targeted cementing zone, operational techniques, and process parameters [12]. These factors have led to the development of different cementing methods, such as the balanced plug technique [15], squeeze cementing [16], two-plug methods [12], off-bottom techniques [17], and dump bailing [12], [18]. This study focuses on the dump bailing method, where cementing involves initially setting a permanent mechanical bridge plug below the designated cementing zone. A bailer containing the cement slurry is then lowered into the wellbore, which is typically filled with wellbore fluid, often water in Canada. The cement slurry is later released or injected onto the bridge plug. From a fluid mechanics stance, this process can be considered as the release or injection of a dense suspension fluid, such as cement paste, into a Newtonian fluid within a closed-end pipe, representing the wellbore casing and bridge plug. The combination of various parameters, including geometrical characteristics, fluid properties, and operational conditions, makes studying this process under different scenarios particularly challenging. Given these complexities, this work aims to investigate buoyant miscible suspension fluid injection into a closed-end pipe filled with quiescent Newtonian fluid.

Several studies have investigated buoyant miscible displacement flows relevant to the dump-bailing method. Akbari and Taghavi [5] conducted experiments on the injection of a heavy Newtonian fluid into a quiescent lighter Newtonian fluid within an inclined, closed-end pipe, simulating the dump-bailing process. They identified distinct flow patterns, including a buoyant jet at the initial stage, mixing near the inlet at high

injection rates, slumping due to transverse buoyancy stresses, and fluid return. Further research by Akbari and Taghavi [18] highlighted that reducing the dumping height and increasing the viscosity and density of the injected fluid improved placement efficiency, while the flow in the gap between the bailer and casing remained unaffected by fluid dynamics in the targeted zone. Following research [19], [20] studied the impact of the non-Newtonian properties of cement slurries. Considering the shear thinning behavior of cement slurry, both experimental and numerical investigations demonstrated fluid separation when highly viscous fluids were injected [21]. Moreover, when treating the cement slurry as a high-yield stress fluid, they identified various flow regimes, including breakup, coiling, and bulging under vertical configurations. Faramarzi et al. [22] expanded this research by investigating moderate to low yield stress fluids in both inclined and vertical configurations, identifying four primary regimes: stable slumping, unstable slumping, separation, and mixing, with stable slumping emerging as the most favorable due to its minimal mixing and stable interface.

The cement slurry, including cement particles, can be categorized as a particle-laden fluid or suspension. Extensive research has studied the dynamics of such suspensions, with a focus on key phenomena such as turbidity currents [23], [24] and debris flows across inclined surfaces [25], [26]. Despite extensive research, the behavior of buoyant particulate suspensions injected or released into other fluids has received limited attention, particularly in dynamically active systems where fluid motion influences suspension dynamics. Existing studies primarily focus on neutrally buoyant particles, where the particle density closely matches that of the fluid medium. Findings indicate that higher injection rates enhance turbulence, thereby reducing particle settling [27]–[30]. Furthermore, increasing the inclination angle toward the vertical direction promotes turbulence, further reducing particle deposition [31], [32]. In this context, this study examines the injection of a heavy suspension into a closed-end pipe filled with lighter Newtonian fluid, investigating the effects of inclination angle, injection rate, and initial particle concentration on flow dynamics. Advanced non-intrusive visualization techniques and data processing methods are employed to quantify key factors, including the position of the suspension front, concentration distributions, and placement efficiency, using a mixing index.

The structure of this paper is organized as follows: Section 2 outlines the methodology, providing a detailed overview of the experimental setup and the procedure employed. Section 3 discusses experimental results, focusing on the effects of initial particle volume fraction, inclination angle, and injection rate. Finally, Section 4 provides a summary of the key findings.

II. Methodology

In this study, experiments were conducted using a scaled-down experimental setup consisting of two transparent pipes connected eccentrically, as shown in Fig. 1. The inner pipe, with a diameter of 1.27 cm and an outer diameter of 2.54 cm, represents the bailer used for injecting the suspension. The outer pipe, with an inner diameter of 3.81 cm, represents the wellbore casing. The setup includes a movable piston inside the inner pipe, which adjusts the falling height from the injection inlet to the piston, defining the medium of interest in this study, as highlighted by the pink dashed line in Fig. 1. The entire setup is mounted on a rotatable structure, facilitating the study of buoyant suspension injection at different inclination angles. A gate valve installed at the end of the inner pipe isolates the injection fluid from the ambient fluid. Additional details regarding the experimental setup can be found in [22].

To conduct an experiment using this setup, the inner pipe is initially filled with the suspension, while the outer pipe is cleaned and then filled with deionized water. The two fluids are separated by a gate valve installed at the end of the inner pipe. The experiment begins by opening the gate valve and turning on the pump at a predefined flow rate to transfer the suspension. In this work, dosing pumps (RJ30) are used to handle the suspension from a bucket, where a mixer (IKA Werke EUROSTAR POWER) continuously stirs the suspension to prevent particle settling and maintain a homogeneous mixture.

The suspension preparation starts with adding a designated quantity of ink (0.8 g/l) to a 99.7% glycerin solution, characterized by a density of 1260 kg/m^3 and a viscosity of 1400 cp. The mixture is subsequently mixed at 350 rpm. A predetermined quantity of solid particles is incrementally introduced to the solution. The solid particles utilized are soda-lime microsphere glass beads from Composition Material Co., Inc. with an average diameter of around 70 μm and a density of about 2500 kg/m^3. These beads range in diameter from 44 to 88 μm (170 to 325 US mesh). To meet the research aims, we made two suspension solutions with initial particle volume fractions of 5% and 10%. To verify the initial particle concentration, the density of each prepared suspension was measured at least three times using a digital density meter (Anton Paar DMA 35N). We then compared the measured densities with the theoretical values based on expectations [33], [34], which are expressed as:

$$\hat{\rho}_H(\phi_o) = \hat{\rho}_p\phi_o + \hat{\rho}_f(1-\phi_o), \tag{1}$$

where $\hat{\rho}_H$ is the suspension density, ϕ_o represents the initial volume fraction of solid particles, $\hat{\rho}_p$ is the density of the solid particles, and $\hat{\rho}_f$ refers to the density of the carring fluid. The viscosity of the suspension ($\hat{\mu}_H$) can also be determined using Newtonian rheology principles [33], as given by:

$$\hat{\mu}_H(\phi_o) = \hat{\mu}_f(1-\frac{\phi_o}{\phi_j})^{-2}, \tag{2}$$

where ϕ_j represents the jamming volume fraction, which has been reported to be 0.61 for spherical particles [33], [35]. The viscosity of the carrier fluid, $\hat{\mu}_f$, was measured using a digitally controlled rheometer (DHR-3, TA Instruments), which provides shear stress and shear rate measurements.

Prepared suspensions are dyed with black ink (Fountain Pen India Black) at a concentration of 0.8 g/L in deionized water

before adding particles. LEDs are positioned behind the pipe, as shown in Fig. 1, with diffusive panels in between to ensure uniform lighting. The interfacial flow within the region of interest is recorded using a high-speed black-and-white camera (Basler ACA2040). Before each experiment, light absorption calibrations are also performed using reference images of the pipe filled separately with transparent and dyed fluids. These images are used to calculate normalized concentration fields via the Beer-Lambert law [21]. Image processing is carried out using a custom MATLAB code to extract concentration fields and interfacial flow dynamics. Flow rates are determined by tracking pump output and measuring the fluid volume expelled from the outer pipe.

Table I presents the dimensional parameters, denoted by a circumflex, along with their respective ranges used in this study. To enable the application of experimental findings to industrial scales, dimensionless parameters were derived from these dimensional values. As shown in Table II, the experiments were conducted at a high Péclet number (Pe), where particle self-diffusion becomes negligible, consistent with Espin and Kumar's findings [36] for $\frac{Pe}{H^2} \gg 1$. Under these conditions, settling and shear-induced migration are the primary diffusion mechanisms [33], [36]. The study also explores the injection of dense suspensions with initial particle volume fractions (ϕ_o) of 5% and 10%, calculated as the ratio of particle volume ($\hat{V}_p$) to carrying fluid volume ($\hat{V}_c$). Moreover, the influence of inclination angles at 15° and 70° was examined, representing near-horizontal and near-vertical configurations. To generalize the results, lengths, velocities, and time were nondimensionalized using $\hat{D}$, $\hat{V}_0$, and $\hat{D}/\hat{V}_0$, respectively.

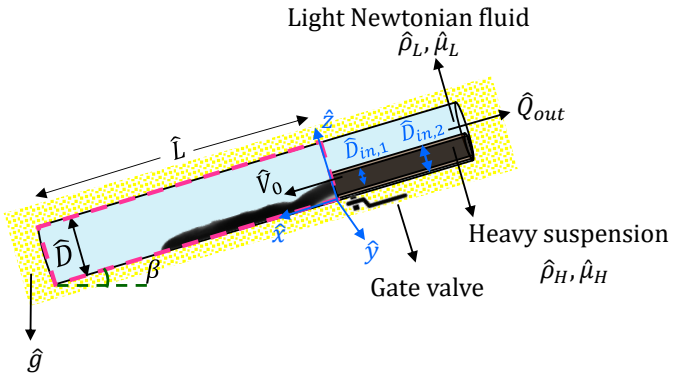

Figure. 1. Schematic of the experimental setup, with the pink dashed line representing the medium of interest in this study.

III. Results and Discussion

This section presents the results of suspensions injected in a prefilled pipe containing deionized water, examining the effects of initial particle volume fraction, injection rate, and inclination angle. We begin with a general overview of flow development and patterns observed in the experiments,

TABLE. I
DIMENSIONAL PARAMETERS USED IN OUR EXPERIMENTS, ALONG WITH THEIR CORRESPONDING RANGES.

Parameter	Name	Range or value
$\hat{D}$	Inner diameter of outer pipe	3.81 (cm)
$\hat{D}_i$	Inner diameter of bailer	1.27 (cm)
$\hat{D}_o$	Outer diameter of bailer	2.54 (cm)
$\hat{H}$	Dumping height	0.46 (m)
$\hat{V}_0$	Injection velocity	70-100 (mm/s)
$\hat{\rho}_f$	Carrying fluid density	1260 (kg/m^3)
$\hat{\rho}_H$	Heavy suspension fluid density	1322, 1384 (kg/m^3)
$\hat{\rho}_L$	Light Newtonian fluid density	998 (kg/m^3)
$\hat{\mu}_f$	Carrying fluid viscosity	1.4 (Pa.s)
$\hat{\mu}_H$	Heavy suspension fluid viscosity	1.66, 2 (Pa.s)
$\hat{\mu}_L$	Light Newtonian fluid viscosity	0.001 (Pa.s)
$\hat{D}_E$	Einstein diffusivity [36]	$\sim 10^{-18}$ (m^2/s)
$\hat{g}$	Gravitational acceleration	9.81 (m/s^2)
$\hat{d}_p$	Particle size	~ 70 (μm)
$\hat{\rho}_p$	Particle density	2500 (kg/m^3)

TABLE. II
DIMENSIONLESS PARAMETERS USED IN OUR EXPERIMENTS, ALONG WITH THEIR CORRESPONDING RANGES.

Parameter	Name	Definition	Range or value
H	Aspect ratio	$\frac{\hat{H}}{\hat{D}}$	12.07
D_i	Diameter ratio	$\frac{\hat{D}_i}{\hat{D}}$	1/3
Re	Reynolds number	$\frac{(\hat{\rho}_H+\hat{\rho}_L)\hat{V}_0\hat{D}}{2\hat{\mu}_H}$	1.88-3.03
At	Atwood number	$\frac{\hat{\rho}_H-\hat{\rho}_L}{\hat{\rho}_H+\hat{\rho}_L}$	0.14,0.16
Fr	Froude number	$\frac{\hat{V}_0}{\sqrt{At\hat{g}\hat{D}}}$	0.3-0.44
M	Viscosity ratio	$\frac{\hat{\mu}_L}{\hat{\mu}_H}$	0.0005, 0.0006
Pe	Péclet number	$\frac{\hat{V}_0\hat{D}}{\hat{D}_E}$	$\sim 1 \times 10^{15}$
β	Inclination	-	15 & 70°
ϕ_o	Initial volume fraction of particles	$\frac{\hat{V}_p}{\hat{V}_p+\hat{V}_c}$	0.05, 0.1
D_p	Particle diameter ratio	$\frac{\hat{d}_p}{\hat{D}}$	0.0018

followed by an analysis of how each factor influences concentration profiles, front dynamics, and placement efficiency.

A. General observation and effect of initial volume fraction of particles

The injection of suspension into quiescent water in a closed-end pipe can result in varying flow patterns as the flow develops. Fig. 2 shows images from two experiments conducted under identical conditions, differing only in the initial particle volume fraction. Initially, a short buoyant jet forms as the suspension begins to flow. The injected suspension then reaches the lower pipe wall due to transverse buoyant stresses, causing the suspension fluid to slump beneath the ambient fluid. This behavior is driven by the high-density difference and the presence of particles in the suspension.

Fig. 3 shows the spatiotemporal diagram of suspension injection for the experiment in Fig. 2. It illustrates the depth-averaged concentration field of the injected suspension in the dimensionless x–t plane, from the start of the experiment

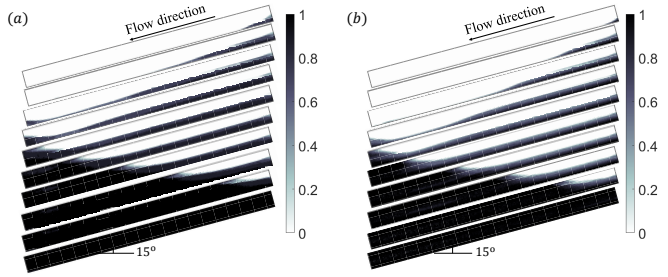

Figure. 2. Experimental snapshots: (a) an experiment with $Re = 3.03$, $\beta = 15°$, $Fr = 0.44$, and $\phi_o = 0.05$, $M = 0.0006$; (b) an experiment with $Re = 2.6$, $\beta = 15°$, $Fr = 0.4$, and $\phi_o = 0.10$, $M = 0.0005$. TThe colorbars represent the concentration of the heavy suspension fluid. The dimensionless field of view is 1×12.

until the pipe is filled. The diagram provides insights into flow dynamics, such as the front velocity, marked by the boundary between colored and white regions, and the average front velocity, indicated by the pink dashed lines in Fig. 3. The results show that the average front velocity is higher in the experiment with a lower initial particle volume fraction compared to the one with a higher fraction. The diagram also highlights the flow pattern from initiation to complete pipe filling. The region between the pink and yellow dashed lines represents the suspension slumping, characterized by nearly uniform concentration. The concentration profiles are almost identical for both experiments. The yellow dashed line marks the average backflow front velocity, indicating when the viscoplastic fluid reaches and fills the pipe's end. Both experiments alomst show similar backflow front velocities, with the lower initial volume fraction case being slightly higher. Below the yellow dashed lines, the pipe-filling process is also depicted. Both experiments demonstrate uniform, high-quality concentration placement in this region. Finally, the experiments reveal that the case with the lower initial particle volume fraction fills the pipe faster than the case with the higher volume fraction.

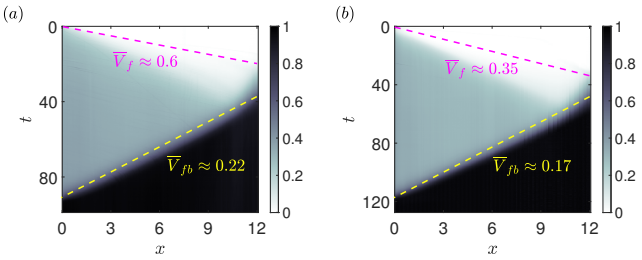

Figure. 3. Spatiotemporal diagram of the depth-averaged concentration field on the dimensionless x-t plane, corresponding to the experiments shown in Fig. 2. The pink dashed line represents the average front velocity, while the yellow dashed line indicates the backflow front velocity. The colorbars depict the depth-averaged concentration of the heavy suspension fluid.

B. Effect of inclination angle

Fig. 4 shows 10 snapshots and a spatiotemporal diagram for an experiment conducted at $\beta = 70°$. The findings reveal that increasing the inclination angle leads to a more unstable slumping flow, where the suspension overcomes eccentricity and settles beneath the ambient Newtonian fluid. At higher inclination angles, concentration profile variations become more pronounced, resulting in increased mixing between the two fluids. Due to the significant density difference and particle presence, the suspension descends rapidly, sometimes leading to suspension separation. When separation occurs, the detached portions deform, transitioning from filament-like shapes to irregular fragments. These fragments eventually settle on the piston, which acts as a mechanical bridge plug, displacing the water. As fragments accumulate, a counterflow develops, gradually filling the pipe from the piston toward the gate valve.

The average front velocity at $\beta = 70°$ is $\overline{V}_f \approx 1.5$, significantly higher than $\overline{V}_f \approx 0.35$ observed at lower inclination angles. This increase is attributed to reduced interface height and the occurrence of suspension separations. Conversely, the backflow front velocity decreases at higher inclination angles, indicating that the interface height during slumping diminishes as the inclination increases from 15° to 70°, as discussed. Moreover, the pipe filling time, expressed in dimensionless terms, rises with increasing inclination angles.

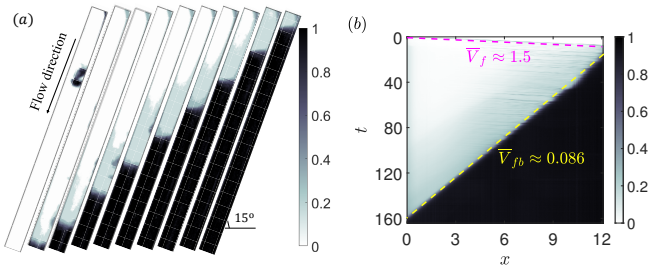

Figure. 4. (a) Experimental snapshots from an experiment with $Re = 2.38$, $\beta = 70°$, $Fr = 0.37$, and $\phi_o = 0.1$, $M = 0.0005$. The dimensionless field of view is 1×12. (b) Corresponding spatiotemporal diagram of the depth-averaged concentration field on the dimensionless x-t plane.

C. Effect of injection rate

Fig. 5 presents a snapshot and spatiotemporal diagram of an experiment with identical properties to Fig. 4, except for a lower injection rate. Despite the reduced injection velocity, the results indicate similar values for $\overline{V}_f$. Interestingly, $\overline{V}_f$ for the lower injection rate exceeds that of the higher injection rate case. Alike, $\overline{V}_{fb}$ follows a similar trend, being larger at the lower injection rate. Moreover, the results show that under varying injection velocities, a consistent pattern occurs in the slumping and filling processes. The findings also reveal that the dimensionless pipe filling time decreases as the injection rate is reduced.

D. Displacement efficiency

Quantifying the quality of fluid placement over time is practically significant. One approach involves analyzing concentration profiles, where a uniformly high suspension concentration indicates effective displacement. To present and

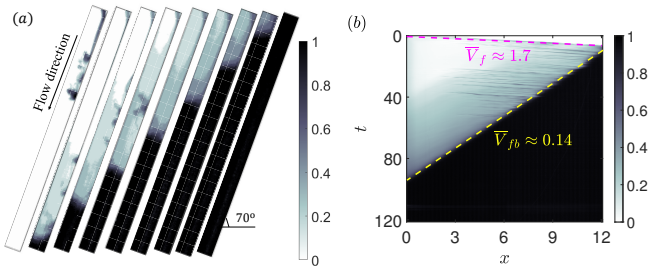

Figure. 5. (a) Experimental snapshots from an experiment with $Re = 1.88$, $\beta = 70°$, $Fr = 0.29$, and $\phi_o = 0.1$, $M = 0.0005$. The dimensionless field of view is 1×12. (b) Corresponding spatiotemporal diagram of the depth-averaged concentration field on the dimensionless x-t plane.

compare different experiments, mixing indices are employed to assess the mixing quality between the injected and ambient fluids. In this study, a mixing index based on 2D camera images is defined as follows [22]:

$$MI(x, y, t) = \frac{\sum_{i=1}^{N} \sum_{j=1}^{M} (1 - C(x, y))}{N \times M}, \tag{3}$$

where $C(x, y)$ denotes the suspension concentration at pixel coordinates (x, y), and N and M represent the number of pixels in the x and y directions containing the suspension. Here, $C(x, y) = 0$ corresponds to the light fluid, and $C(x, y) = 1$ to the heavy fluid. A lower mixing index value, as defined by Eq. 3, indicates more efficient fluid placement.

Fig. 6(a) shows the evolution of the average mixing index ($\overline{MI}$) over time for two experiments with different inclination angles. The solid dark red line represents the higher inclination, while the pink dashed line corresponds to the lower inclination. The results indicate that $\overline{MI}$ is consistently lower for the lower inclination, indicating better fluid placement efficiency. Moreover, the experiment with a lower inclination reaches the ultimate steady $\overline{MI}$ more rapidly than the higher inclination case.

Fig. 6(b) compares the effect of injection rate on $\overline{MI}$ over time. The blue solid line represents the higher injection rate, while the cyan dashed line corresponds to the lower injection rate. Since dimensional parameters have been made dimensionless by $\hat{V}_0$, we use another dimensionless scale to compare the effect of injection rate. In this regard, similar to previous studies, we non-dimensionalize the lengths, velocities, and time by dividing them by $\hat{D}$, the characteristic inertial-buoyant velocity ($\hat{V}_{ib}$), and $\hat{D}/\hat{V}_{ib}$, respectively [18]. The inertial-buoyant velocity, $\hat{V}_{ib}$, is obtained by balancing the buoyant stress ($(\hat{\rho}_H - \hat{\rho}_L)\,\hat{g}\hat{D}$) with the inertial stress ($(\hat{\rho}_H + \hat{\rho}_L)\,\hat{V}_{ib}^2$), as follows:

$$(\hat{\rho}_H - \hat{\rho}_L)\,\hat{g}\hat{D} \sim (\hat{\rho}_H + \hat{\rho}_L)\,\hat{V}_{ib}^2 \quad \Rightarrow \quad \hat{V}_{ib} = \sqrt{At\hat{g}\hat{D}}. \tag{4}$$

The results show that $\overline{MI}$ under the lower injection rate is consistently lower than $\overline{MI}$ with the higher injection rate, indicating that placement efficiency decreases with an increase in the injection rate.

Fig. 6(c) illustrates the evolution of $\overline{MI}$ for experiments with different initial particle volume fractions. The solid dark green line represents the higher initial volume fraction, while the light green dashed line corresponds to the lower initial volume fraction. Initially, the higher volume fraction case exhibits a lower $\overline{MI}$, indicating better fluid placement quality at early times. Over time, however, the mixing index for the lower volume fraction case declines more rapidly, eventually matching the reduction rate of the higher volume fraction case. Furthermore, the experiment with a lower initial particle volume fraction reaches a stable $\overline{MI}$ more quickly.

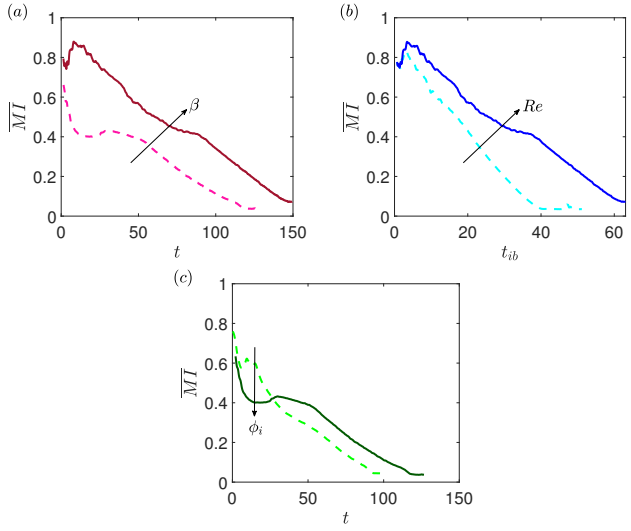

Figure. 6. $\overline{MI}$ vs. time: (a) Effect of inclination angle, with the dark red solid line corresponding to the experiment in Fig. 4 and the pink dashed line corresponding to Fig. 2b. (b) Effect of injection rate, using dimensionless inertial-buoyant time t_{ib} as the time scale. The solid blue line represents Fig. 4, and the cyan dashed line corresponds to Fig. 5. (c) Effect of initial particle volume fraction, with the solid dark green line representing the experiment in Fig. 2b and the light green dashed line representing the experiment in Fig. 2a.

IV. Conclusion

In this study, we experimentally investigated the injection of a heavy suspension into a closed-end pipe filled with a lighter Newtonian fluid, examining the effects of inclination angle, injection rate, and initial particle concentration on flow dynamics. The experiments were conducted using a scaled-down setup simulating cementing operations in oil and gas wells. Advanced non-intrusive visualization techniques and data processing methods were employed to quantify key parameters, including the suspension front position, concentration distributions, and placement efficiency, evaluated through a mixing index. The results indicated that increasing the initial particle volume fraction prolonged the pipe-filling time. In the short term, higher initial particle concentrations improved displacement quality, but over longer periods, lower initial particle concentrations resulted in better placement efficiency. Regarding inclination angle, an increase led to longer filling times and diminished placement quality. Furthermore, reducing the

injection rate enhanced suspension placement efficiency while also decreasing the pipe-filling time. In terms of front velocity, the findings revealed that it decreased with higher initial particle concentrations, increased with greater inclination angles, and showed a slight rise when the injection rate was reduced. This research provides insights into cementing operations in oil and gas wells, particularly for applications such as the dump-bailing method, primary cementing, cementing during hydrocarbon production, and wellbore decommissioning.

ACKNOWLEDGMENT

This research was done at the Univerité Laval. We gratefully acknowledge the financial support provided by PTAC-AUPRF through Grant No. AUPRF2022-000124 and NSERC, Canada through Alliance Grant No. ALLRP577111-22 ("Towards Net-Zero Emissions: mechanics, processes and materials to support risk-based well decommissioning"). We also acknowledge the support provided by the Canada Foundation for Innovation (Grant No. GF130120, GQ130119, and GF525075), the Canada Research Chair (CRC) on Modeling Complex Flows (Grant No. CG125810), and the NSERC Discovery Grant (Grant No. CG109154).

REFERENCES

[1] C. Duan, X. Yang, S. Jiang, C. Zhu, Y. Ma, and T. Fu, "Early stage of externally driven filling of viscous fluids within a microfluidic pore-doublet network," *Physics of Fluids*, vol. 34, no. 2, 2022. (*references*)

[2] P. Bazazi, H. A. Stone, and S. H. Hejazi, "Spongy all-in-liquid materials by in-situ formation of emulsions at oil-water interfaces," *Nature Communications*, vol. 13, no. 1, p. 4162, 2022.

[3] S. K. Veerabhadrappa, J. J. Trivedi, and E. Kuru, "Visual confirmation of the elasticity dependence of unstable secondary polymer floods," *Industrial & Engineering Chemistry Research*, vol. 52, no. 18, pp. 6234–6241, 2013.

[4] W. Liu, F. Larachi, and S. M. Taghavi, "Immiscible non-Newtonian displacement flows in stationary and axially rotating pipes," *Physics of Fluids*, vol. 36, no. 10, 2024.

[5] S. Akbari and S. M. Taghavi, "Injection of a heavy fluid into a light fluid in a closed-end pipe," *Physics of Fluids*, vol. 32, no. 6, 2020.

[6] H. Hassanzadeh, A. Eslami, and S. M. Taghavi, "Positively buoyant jets: semiturbulent to fully turbulent regimes," *Physical Review Fluids*, vol. 6, no. 5, pp. 054501, 2021.

[7] M. Faramarzi-Palangar and A. Mirzaei-Paiaman, "Identifying two-phase flow rock types in CO2-brine systems using TEM-function," *Journal of Petroleum Science and Engineering*, vol. 205, p. 108818, 2021.

[8] M. Faramarzi-Palangar and A. Mirzaei-Paiaman, "Investigating dynamic rock quality in two-phase flow systems using TEM-function: A comparative study of different rock typing indices," *Petroleum Research*, vol. 6, no. 1, pp. 16–25, 2021.

[9] H. Safari, M. Faramarzi-Palangar, S. M. H. Hashemi, O. Neisarifam, and B. Sedaee, "A new approach to 3D saturation height modeling by coupling a capillary pressure model with pore throat size distribution," *Natural Resources Research*, vol. 31, no. 2, pp. 1045–1059, 2022.

[10] M. Faramarzi-Palangar, B. Sedaee, and M. Emami Niri, "A further investigation on the application of critical pore size as an approach for reservoir rock typing," *Journal of Energy Resources Technology*, vol. 143, no. 11, p. 112901, 2021.

[11] S. Lyu and S. M. Taghavi, "Viscoplastic displacements in axially rotating pipes," *Journal of Non-Newtonian Fluid Mechanics*, vol. 284, p. 104353, 2020.

[12] M. Khalifeh and A. Saasen, *Introduction to Permanent Plug and Abandonment of Wells*, Springer, 2020.

[13] M. Faramarzi, S. Akbari, H. Hassanzadeh, M. Hafezi, and S.M. Taghavi, "Plug and Abandonment of Oil and Gas Wells: Experimental Study of Suspension Fluid Placements in a Confined Geometry With Insights Into the Dump Bailing Method," in *Proc. Int. Conf. Offshore Mechanics and Arctic Engineering*, vol. 87868, pp. V008T11A032, 2024, American Society of Mechanical Engineers.

[14] E. Trudel, M. Bizhani, M. Zare, and I. A. Frigaard, "Plug and abandonment practices and trends: A British Columbia perspective," *Journal of Petroleum Science and Engineering*, vol. 174, p. 106417, 2019.

[15] C. Carpenter, "Stinger or tailpipe placement of cement plugs," *Journal of Petroleum Technology*, vol. 66, no. 05, pp. 147–149, 2014.

[16] M. Izadi, E. Chaparian, E. Trudel, and I. Frigaard, "Squeeze cementing of micro-annuli: A visco-plastic invasion flow," *Journal of Non-Newtonian Fluid Mechanics*, vol. 319, p. 105070, 2023.

[17] A. Ghazal and I. Karimfazli, "On the hydrodynamics of off-bottom plug placement: A 2D model problem," *Journal of Petroleum Science and Engineering*, vol. 203, p. 108613, 2021.

[18] S. Akbari and S. M. Taghavi, "Fluid experiments on the dump bailing method in the plug and abandonment of oil and gas wells," *Journal of Petroleum Science and Engineering*, vol. 205, p. 108920, 2021.

[19] S. Akbari and S.M. Taghavi, "From breakup to coiling and buckling regimes in buoyant viscoplastic injections," *Journal of Fluid Mechanics*, vol. 940, p. A42, 2022.

[20] S. Akbari and S.M. Taghavi, "Immersed buoyant viscoplastic injections," *Journal of Non-Newtonian Fluid Mechanics*, vol. 306, p. 104836, 2022.

[21] S. Akbari and S. M. Taghavi, "Buoyant fluid injections at high viscosity contrasts in an inclined closed-end pipe," *Physics of Fluids*, vol. 35, no. 2, 2023.

[22] M. Faramarzi, S. Akbari, and S.M. Taghavi, "Buoyant miscible viscoplastic injections," *Physical Review Fluids*, vol. 9, no. 7, p. 073301, 2024.

[23] R.T. Bonnecaze, H.E. Huppert, and J.R. Lister, "Particle-driven gravity currents," *Journal of Fluid Mechanics*, vol. 250, pp. 339–369, 1993.

[24] E. Meiburg and B. Kneller, "Turbidity currents and their deposits," *Annual Review of Fluid Mechanics*, vol. 42, no. 1, pp. 135–156, 2010.

[25] J. Zhou, B. Dupuy, A.L. Bertozzi, and A.E. Hosoi, "Theory for shock dynamics in particle-laden thin films," *Physical Review Letters*, vol. 94, no. 11, pp. 117803, 2005.

[26] B.P. Cook, A.L. Bertozzi, and A.E. Hosoi, "Shock solutions for particle-laden thin films," *SIAM Journal on Applied Mathematics*, vol. 68, no. 3, pp. 760-783, 2008.

[27] A. Yousefi, P. Costa, F. Picano, and L. Brandt, "On the role of inertia in channel flows of finite-size neutrally buoyant particles," *Journal of Fluid Mechanics*, vol. 955, A30, 2023.

[28] I. Lashgari, F. Picano, W.-P. Breugem, and L. Brandt, "Laminar, turbulent, and inertial shear-thickening regimes in channel flow of neutrally buoyant particle suspensions," *Physical Review Letters*, vol. 113, no. 25, pp. 254502, 2014.

[29] W. Hogendoorn, W.-P. Breugem, D. Frank, M. Bruschewski, S. Grundmann, and C. Poelma, "From nearly homogeneous to core-peaking suspensions: Insight in suspension pipe flows using MRI and DNS," *Physical Review Fluids*, vol. 8, no. 12, p. 124302, 2023.

[30] Y. Chen, E. Otoo, Y. Chen, Z. Xu, X. Li, and Y. Zhou, "Deposition behaviour of inclined momentum sediment-laden jet," *Ocean Engineering*, vol. 278, p. 114399, 2023.

[31] M. C. Lippert and A. W. Woods, "Experiments on the sedimentation front in steady particle-driven gravity currents," *Journal of Fluid Mechanics*, vol. 889, p. A20, 2020.

[32] R. Maurin, J. Chauchat, and P. Frey, "Revisiting slope influence in turbulent bedload transport: consequences for vertical flow structure and transport rate scaling," *Journal of Fluid Mechanics*, vol. 839, pp. 135–156, 2018.

[33] N. Mirzaeian and K. Alba, "Particle-laden exchange flows in inclined pipes," *Physical Review Fluids*, vol. 3, no. 11, p. 114301, 2018.

[34] I. M. Krieger, "Rheology of monodisperse latices," *Advances in Colloid and Interface Science*, vol. 3, no. 2, pp. 111–136, 1972.

[35] S. Saha, D. Salin, and L. Talon, "Low Reynolds number suspension gravity currents," *The European Physical Journal E*, vol. 36, pp. 1–18, 2013.

[36] L. Espín and S. Kumar, "Forced spreading of films and droplets of colloidal suspensions," *Journal of Fluid Mechanics*, vol. 742, pp. 495–519, 2014.